Journal of Alloys and Compounds 689 (2016) 554–563

Contents lists available at ScienceDirect

Journal of Alloys and Compounds

journal homepage: http://www.elsevier.com/locate/jalcom

Electrochemical properties of micron-sized Co_3O_4 hollow powders consisting of size controlled hollow nanospheres

Jin-Sung Park [a], Jung Sang Cho [b], Jong Hwa Kim [c], Yun Ju Choi [d], Yun Chan Kang [a, *]

[a] Department of Materials Science and Engineering, Korea University, Anam-Dong, Seongbuk-Gu, Seoul 136-713, Republic of Korea
[b] Department of Engineering Chemistry, Chungbuk National University, Chungbuk 361-763, Republic of Korea
[c] Daegu Center, Korea Basic Science Institute, 80 Daehakro Bukgu, Daegu 702-701, Republic of Korea
[d] Suncheon Center, Korea Basic Science Institute, Suncheon 540-742, Republic of Korea

ARTICLE INFO

Article history:
Received 6 May 2016
Received in revised form
20 July 2016
Accepted 21 July 2016
Available online 28 July 2016

Keywords:
Kirkendall diffusion
Ostwald ripening
Cobalt oxide
Anode material
Lithium ion battery
Spray pyrolysis

ABSTRACT

Micron-sized Co_3O_4 hollow powders consisting of size controlled hollow nanospheres are prepared by applying Ostwald ripening and Kirkendall effect to the spray pyrolysis process. The Co-C composite powders uniformly dispersed with different sizes of metallic Co nanocrystals are formed by reduction of the cobalt oxide-carbon composite powders prepared using spray pyrolysis. Subsequent oxidation of the Co-C composite powders with filled structures forms the micron-sized Co_3O_4 hollow powders consisting of size controlled hollow nanospheres. The mean sizes of the Co_3O_4 hollow nanospheres oxidized from Co-C composite powders formed at reduction temperatures of 400, 600, and 800 °C are 37, 55, and 73 nm, respectively. The discharge capacities of the Co_3O_4 powders formed from the Co-C composite powders reduced at temperatures of 400, 600, and 800 °C for the 300th cycle are 644, 702, and 660 mA h g^{-1}, respectively, and their capacity retentions calculated from the second cycle are 81, 86, and 84%, respectively. The porous-structured Co_3O_4 powders formed from the Co-C composite powders reduced at 800 °C show slightly better rate performance than those of the other two samples.

1. Introduction

Hollow structured materials with high surface areas and large void volumes have been extensively studied for applications in various fields including energy storage, gas sensing, and catalysis [1–9]. Hollow nanopowders with mean sizes <100 nm and unique properties have been successfully prepared through various liquid solution processes [10–15]. However, nanopowders with high surface areas suffer from particle aggregation due to strong van der Waals forces. Submicron- and micron-sized aggregate microspheres of hollow nanospheres and multi-shelled microspheres, with intact unique properties and ease of handling, could be used in place of hollow nanospheres [16–20].

Nanostructured cobalt oxide materials with various morphologies have been developed for a number of different applications, including energy storage [21–35]. In particular, hollow structured cobalt oxide powders have good characteristics for use as anode materials in lithium-ion batteries (LIBs) [26–35]. Wang et al. synthesized Co_3O_4 multishelled hollow spheres using hydrothermal method, and their double-shelled hollow structures delivered a capacity of 866 mA h g^{-1} over 50 cycles at a current rate of C/5, showing good rate capacity [34]. Park et al. prepared multi-shelled Co_3O_4 yolk-shell microspheres using a large-scale spray drying process, with 6, 5, and 4 shells arising from post-treatment at 300, 400, and 500 °C, respectively. Multi-shell cobalt oxide yolk-shell powders prepared using a simple spray drying process showed superior electrochemical properties, suitable for use as anode materials for LIBs [35].

In recent years, microspheres and nanofibers consisting of hollow nanospheres were successfully prepared by applying the Kirkendall effect [36–39]. Filled-structured microspheres and nanofibers transformed into hollow nanospheres aggregates by a two-step post-treatment process. Cho et al. synthesized novel structures denoted as bubble–nanorod composites, composed of nanosized hollow Fe_2O_3 spheres uniformly dispersed in an amorphous carbon matrix by introducing Kirkendall effect during electrospinning [38]. The synergetic effects between hollow nanospheres and the carbon matrix resulted in superior cycling and rate performance of the bubble–nanorod-structured Fe_2O_3-C nanofibers. Cho et al. employed Kirkendall effect and Ostwald

* Corresponding author.
E-mail address: yckang@korea.ac.kr (Y.C. Kang).

http://dx.doi.org/10.1016/j.jallcom.2016.07.233
0925-8388/

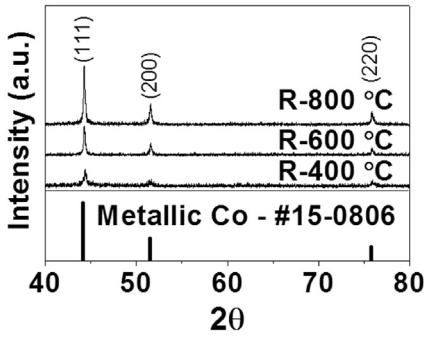

Fig. 1. XRD patterns of the Co-C composite powders reduced at different temperatures.

ripening in tandem to prepare uniquely-structured NiO aggregates. The NiO-C composite powder prepared by one-pot spray pyrolysis was transformed into micron-scale spherical and hollow-structured NiO aggregates after a second-step post-treatment process [39].

In this study, Co_3O_4 powders consisting of size controlled hollow nanospheres were prepared by applying Kirkendall effects to the spray pyrolysis process. The temperature of the first post-treatment process (under a reducing atmosphere) determined the size of the hollow nanospheres formed by Kirkendall effect during the second post-treatment process (under oxidative conditions). The lithium-ion storage properties of these Co_3O_4 powders were also investigated.

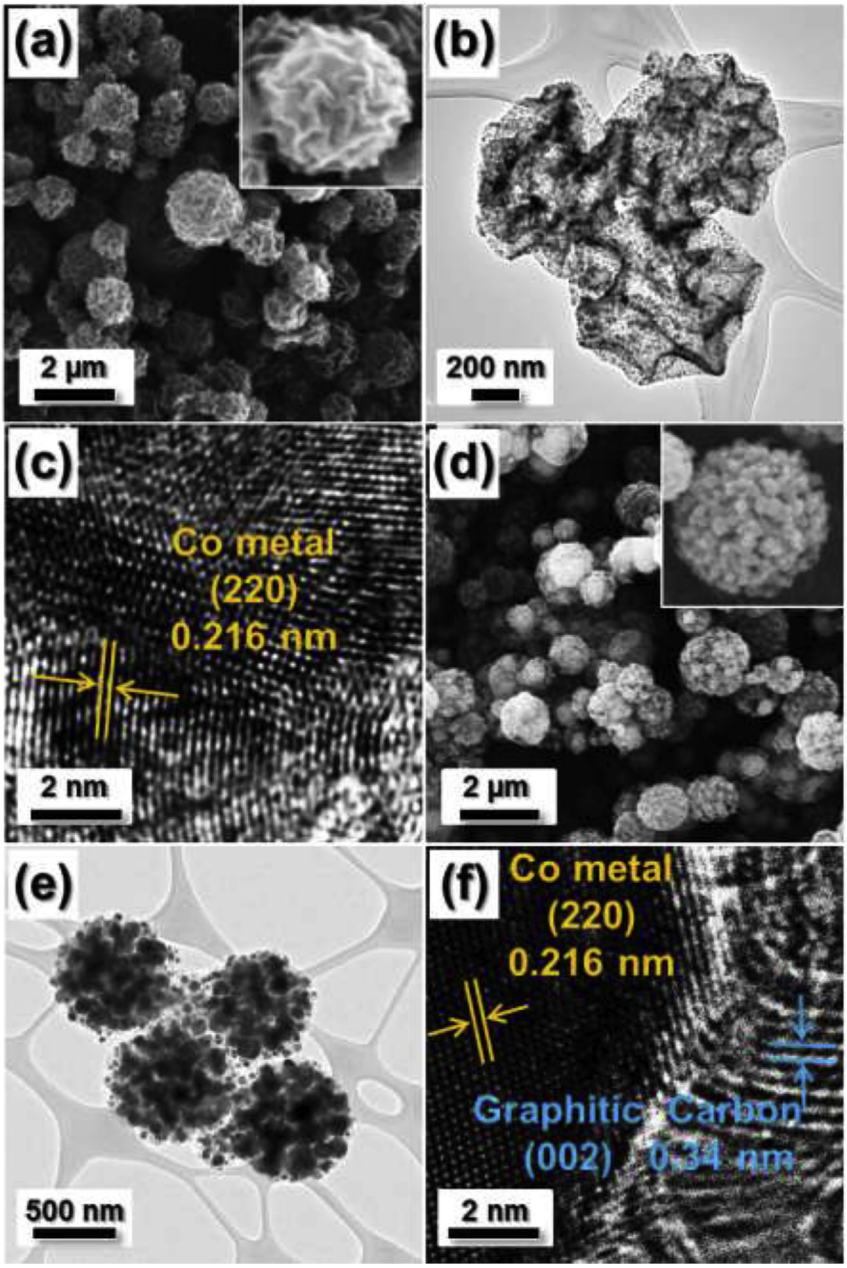

Fig. 2. Morphologies of the Co-C composite powders obtained by reduction of the CoO-carbon composite powders at temperatures of 400 and 800 °C under 10% H_2/Ar gas: (a) SEM image and (b,c) TEM images of the powders reduced at 400 °C and (d) SEM image and (e,f) TEM images of the powders reduced at 800 °C.

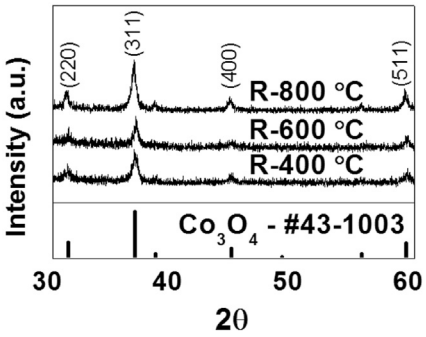

Fig. 3. XRD patterns of the Co_3O_4 powders with size controlled hollow nanospheres.

2. Experimental section

2.1. Sample preparation

Co_3O_4 powders consisting of size controlled hollow nanospheres were prepared by spray pyrolysis and the following two-step post-treatment process. The CoO-carbon composite powders were prepared by spray pyrolysis from a spray solution of cobalt nitrate hexahydrate [$Co(NO_3)_26H_2O$, Junsei] and polyvinylpyrrolidone (PVP) [$(C_6H_9NO)_n$, M_w-40,000, Aldrich]. The spray pyrolysis system used in this study is described in our previous reports. The flow rate of the N_2 carrier gas was fixed at 5 L min^{-1}. The reactor temperature was maintained at 400 °C. The concentrations of cobalt nitrate hexahydrate and PVP dissolved in distilled

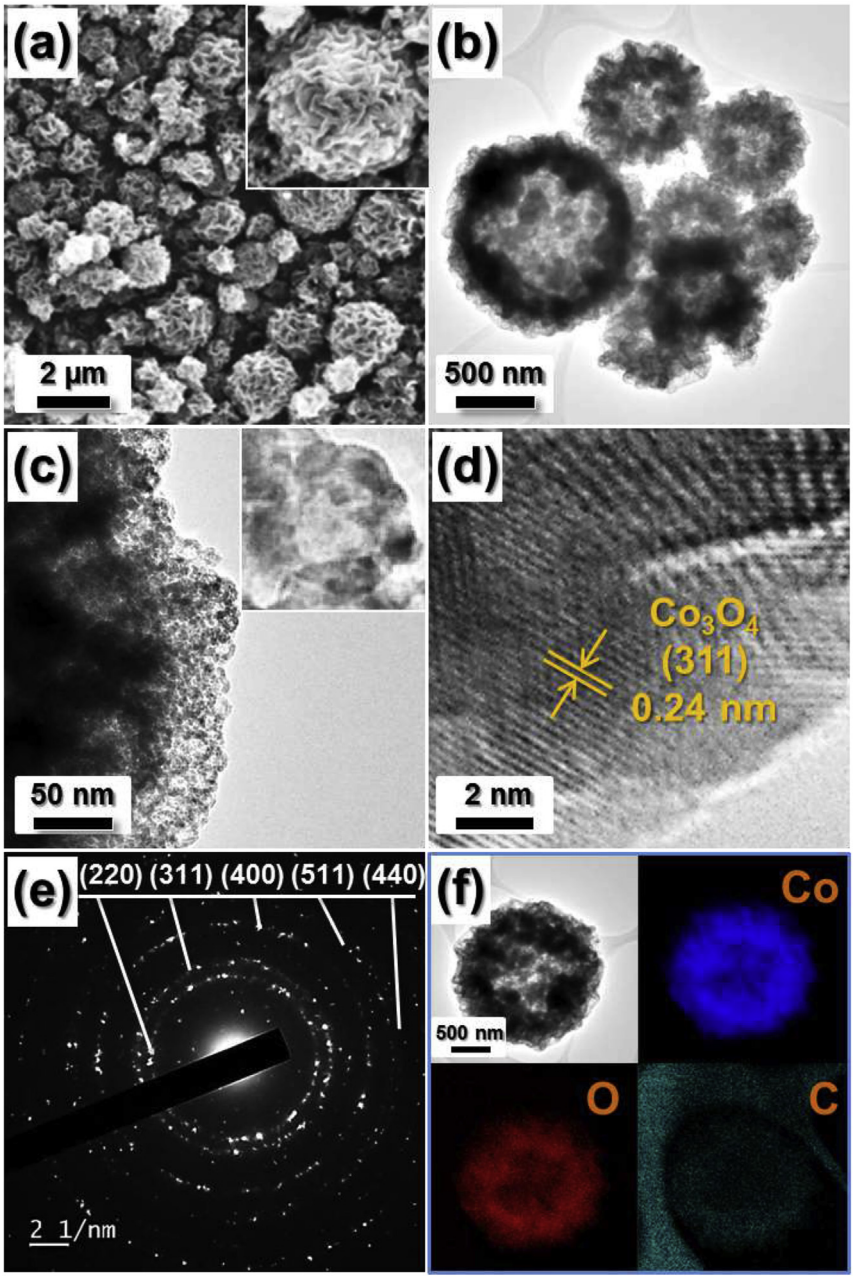

Fig. 4. Morphologies, SAED pattern, and elemental mapping images of the Co_3O_4 powders formed from the Co-C composite powders reduced at 400 °C: (a) SEM image, (b,c) TEM images, (d) HR-TEM image, (e) SAED pattern, and (f) elemental mapping images.

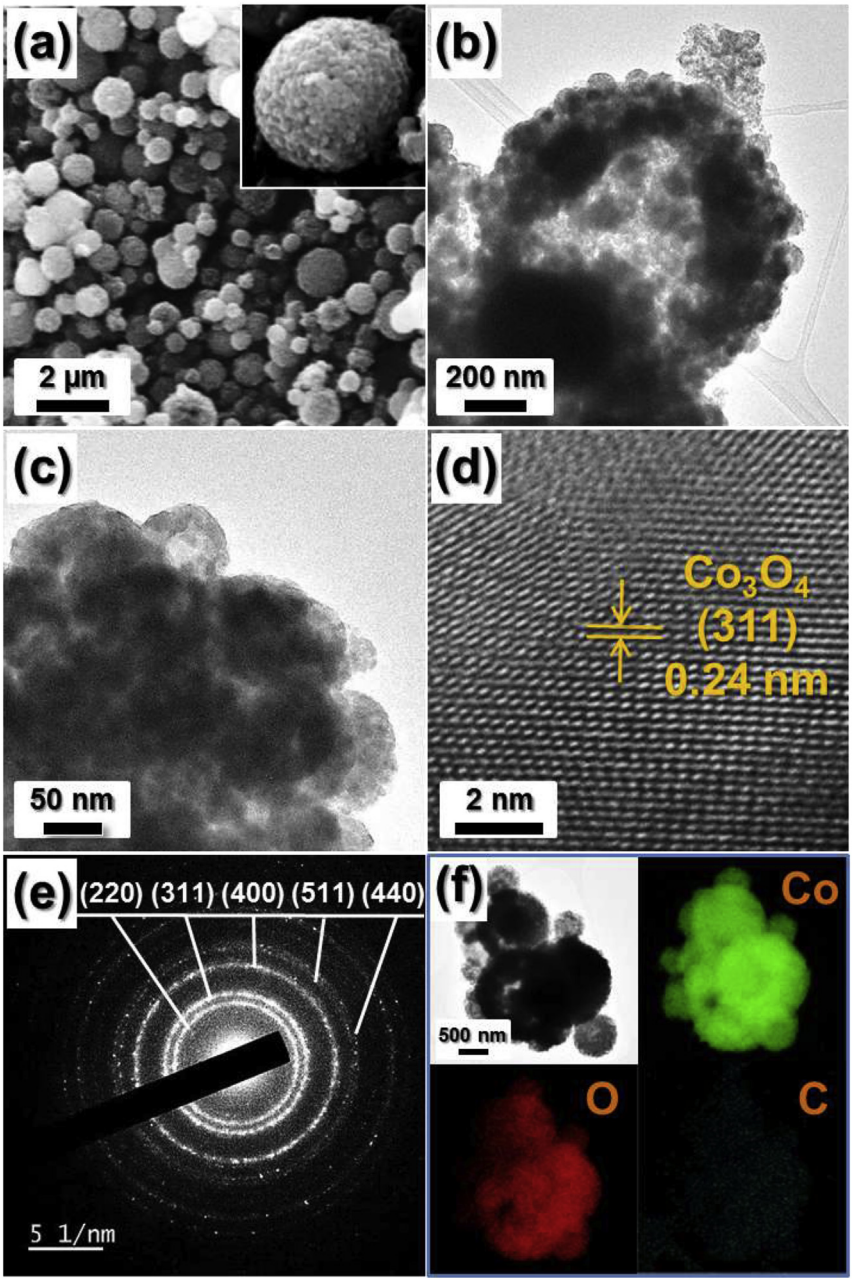

Fig. 5. Morphologies, SAED pattern, and elemental mapping images of the Co_3O_4 powders formed from the Co-C composite powders reduced at 600 °C: (a) SEM image, (b,c) TEM images, (d) HR-TEM image, (e) SAED pattern, and (f) elemental mapping images.

water to prepare the spray solution were 0.05 M and 20 g L^{-1}, respectively. The CoO-carbon composite powders prepared by one-pot spray pyrolysis were post-treated at 400, 600, and 800 °C under a 10% H_2/Ar reducing atmosphere for 10 h to produce the Co-carbon composite powders. The Co-carbon composite powders were post-treated at 400 °C under an oxidizing air atmosphere for 12 h to produce the carbon-free Co_3O_4 powders.

2.2. Characterization techniques

The microstructure of the Co_3O_4 powders was observed using field emission scanning electron microscopy (FE-SEM, Hitachi, S-4800) and field emission transmission electron microscopy (TEM, JEOL, JEM-2100F). In addition, their crystal structures were evaluated with X-ray diffraction (XRD, X'Pert PRO MPD) using Cu K_α radiation ($\lambda = 1.5418$ Å) at the Korea Basic Science Institute (Daegu). The surface area of the powders was determined with the Brunauer–Emmett–Teller (BET) method, using N_2 as the adsorbate gas. Thermogravimetric analysis (TGA) was performed with a Pyris 1 TGA (Perkin Elmer, temperature range = 25–650 °C, heating rate = 10 °C min^{-1}, static air atmosphere).

2.3. Electrochemical measurements

The electrochemical properties of the powders were analyzed by constructing 2032-type coin cells. The anode was prepared by mixing the active material, carbon black, and sodium carboxymethyl cellulose (CMC) in a weight ratio of 7:2:1. Li metal and microporous

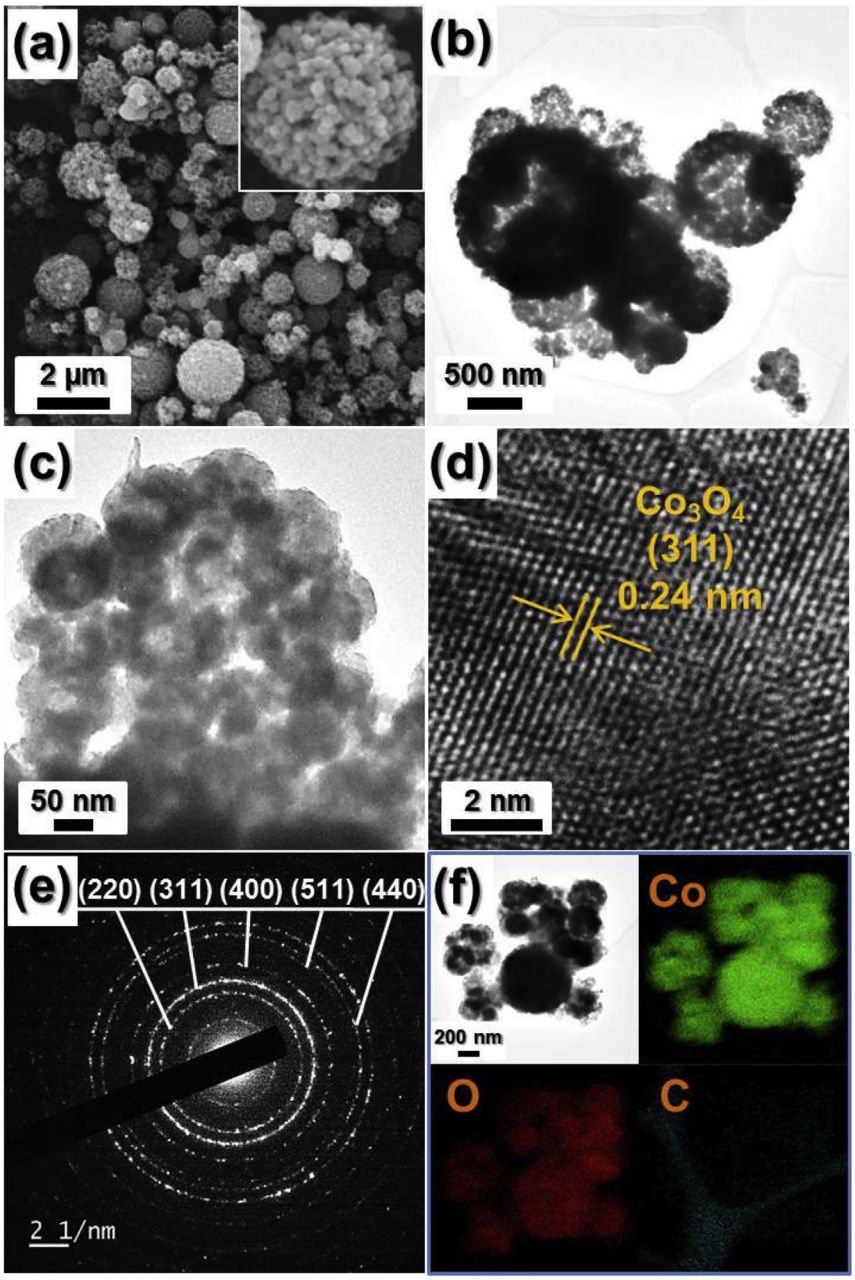

Fig. 6. Morphologies, SAED pattern, and elemental mapping images of the Co_3O_4 powders formed from the Co-C composite powders reduced at 800 °C: (a) SEM image, (b,c) TEM images, (d) HR-TEM image, (e) SAED pattern, and (f) elemental mapping images.

polypropylene film were used as the counter electrode and separator, respectively. The electrolyte was created by dissolving 1 M of $LiPF_6$ in a mixture of fluoroethylene carbonate and dimethyl carbonate (FEC/DMC, 1:1 v/v). The discharge/charge characteristics of the samples were investigated by cycling over a potential range of 0.001–3 V at various current densities. Cyclic voltammograms were measured at a scan rate of 0.1 mV s^{-1}. The size of the negative electrode containing Co_3O_4 powders was 1.25 cm × 1.25 cm, and the mass loading was approximately 0.86 mg cm^{-2}.

3. Results and discussion

The morphologies of the cobalt oxide-carbon composite powders prepared by one-pot spray pyrolysis are shown in Fig. S1. The decomposition of cobalt nitrate and carbonization of polyvinylpyrrolidone (PVP) under N_2 formed cobalt oxide-carbon composite powders with cubic-phase CoO as shown in Fig. S2. Scanning electron microscopy (SEM) images of the cobalt oxide-carbon composite powders shown in Fig. S1a and b revealed spherical shapes and waved structures. The transmission electron microscopy (TEM) images shown in Fig. S1c and d revealed filled structures with ultrafine nanocrystals dispersed within the carbon matrix. The elemental mapping images shown in Fig. S1e revealed uniform distributions of the Co and C components all over the composite powder. The CoO-carbon composite powders were post-treated at 400, 600, and 800 °C under 10% H_2/Ar gas to form the metallic cobalt-C composite powders. The X-ray diffraction (XRD) patterns shown in Fig. 1 confirmed the formation of Co-C composite

powders by a complete reduction of CoO into metallic Co, independent of the reduction temperature. The mean crystallite sizes of the metallic Co of the Co-C composite powders post-treated at 400, 600, and 800 °C as calculated by Scherrer's equation were 37, 39, and 45 nm, respectively. The crystal growth of metallic Co occurred at high reduction temperatures.

The morphologies of the Co-C composite powders post-treated at 400 and 800 °C are shown in Fig. 2. The spherical shapes and filled inner structures of the precursor powders were maintained even after reduction. Additionally, the carbon component prevented aggregation of the powders during the reduction process. The Co-C composite powders post-treated at 400 °C had ultrafine Co nanocrystals below 30 nm dispersed within the amorphous carbon matrix as shown by the TEM images in Fig. 2b and c. However, the TEM images of the Co-C composite powders post-treated at 800 °C shown in Fig. 2e revealed grown Co nanocrystals above 66 nm. The Co nanocrystals shown in Fig. 2f were uniformly coated with graphitic carbon formed by the metallic cobalt catalyst.

The Co-C composite powders obtained at various reduction temperatures were post-treated at 400 °C under ambient air. The XRD patterns of the powders shown in Fig. 3 revealed the pure crystal structure of the cubic Co_3O_4 phase. Complete oxidation of metallic Co into Co_3O_4 occurred during the oxidation process, irrespective of the metallic Co nanocrystal sizes. However, the XRD patterns with broad peaks indicated the formation of ultrafine Co_3O_4 nanocrystals by oxidation.

The morphologies of the cobalt oxide powders formed by oxidation are shown in Figs. 4–6. The spherical morphologies and non-aggregation characteristics of the Co-C composite powders formed at various reduction temperatures were maintained after oxidation to form the cobalt oxide powders shown in the SEM images in Figs. 4a, 5a and 6a. However, the inner structures of the powders were strongly changed after oxidation. The low resolution TEM images shown in Figs. 4b, 5b and 6b revealed hollow-structured cobalt oxide powders. The filled-structured Co-C composite powders transformed into the hollow-structured Co_3O_4 powders after oxidation. The Co component located within the center region moved to the outer region during oxidation by a well-known Ostwald ripening process [40–42]. The Co_3O_4 nanocrystals initially formed near the surface of the Co-C composite powders, and grew by consuming the Co component located in the center region of the powders. The micron-sized hollow powders consisted of hollow-structured ultrafine nanopowders as shown by TEM in Figs. 4c, 5c and 6c. The ultrafine Co nanocrystals were transformed into hollow-structured Co_3O_4 nanospheres by a well-known nanoscale Kirkendall diffusion process [43]. Small Co cations diffused more rapidly to the surface of the cobalt oxide shell than the oxygen gas diffused inward, thereby resulting in the formation of empty voids. The size of hollow-structured Co_3O_4 nanospheres was dependent on the size of metallic Co nanocrystals. Therefore, higher reduction temperatures resulted in Co_3O_4 powders consisting of larger-sized Co_3O_4 hollow nanospheres. The mean sizes of the Co_3O_4 hollow nanospheres consisting of powders formed from Co-C composite powders reduced at 400, 600, and 800 °C were 37, 55, and 73 nm, respectively. The high resolution TEM images shown in Figs. 4d, 5d and 6d revealed clear lattice fringes separated by 0.24 nm, which corresponds to the (311) crystal plane of cubic Co_3O_4 phase [44]. The SAED patterns shown in Figs. 4e, 5e and 6e confirmed the formation of phase-pure Co_3O_4 powders by oxidation. Complete elimination of the carbon component occurred during the oxidation process to form the bare Co_3O_4 powders as shown in the elemental mapping images in Figs. 4f, 5f and 6f. The thermogravimetric (TG) curve of the Co_3O_4 powders formed from the Co-C composite powders reduced at 400 °C (Fig. 7a) also confirmed the complete elimination of carbon during the oxidation process. The N_2 adsorption and desorption isotherms and BJH pore size distributions of the Co_3O_4 powders formed from the Co-C composite powders obtained at different reduction temperatures are shown in Fig. 7b and c, respectively. The Brunauer–Emmett–Teller (BET) surface areas of the Co_3O_4 powders formed from the Co-C composite powders reduced at 400, 600, and 800 °C were 4.8, 12.6, and 17.0 $m^2 g^{-1}$, respectively. The well-developed mesopores of the Co_3O_4 powders formed from the Co-C composite powders reduced at 800 °C (Fig. 7c) resulted in a higher BET surface area. The hollow-structured Co_3O_4 nanospheres consisting of micron-sized powders formed by nanoscale Kirkendall diffusion process had a

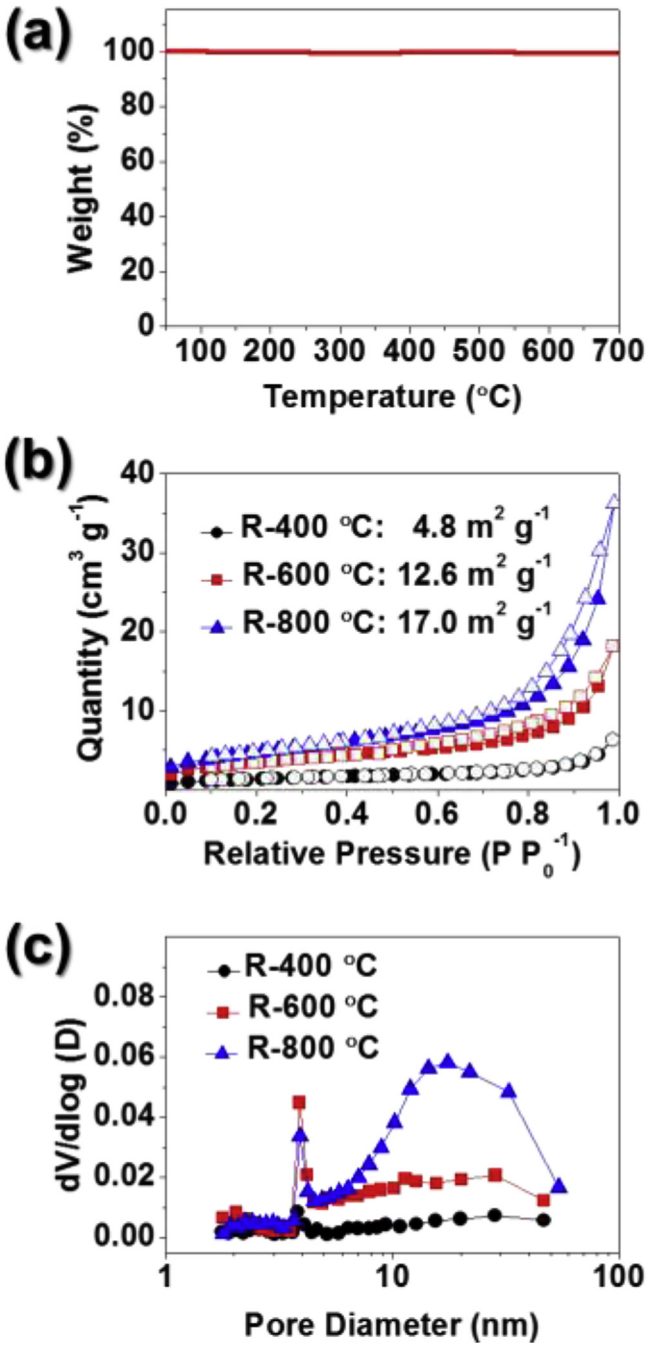

Fig. 7. Characteristics of the Co_3O_4 powders with size controlled hollow nanospheres: (a) TG curve, (b) N_2 adsorption-desorption isotherms, and (c) pore size distributions.

gas impermeable dense shell structure. Therefore, the differences in BET surface areas and BJH pore size distributions of the powders formed from the Co-C composite powders were due to the different networking structures of the Co_3O_4 hollow nanospheres. The oxidation of Co-C composite powders consisting of large-sized metallic Co nanocrystals formed porous Co_3O_4 powders, in which large-sized Co_3O_4 hollow spheres were loosely connected. The formation scheme of the Co_3O_4 powders consisting of size controlled hollow nanospheres is described in Scheme 1.

The electrochemical Li-ion charge and discharge behaviors of the Co_3O_4 powders consisting of size controlled hollow nanospheres were investigated by cyclic voltammetry (CV) and galvanostatic discharge–charge cycling in the voltage range of 0.001–3 V versus Li/Li^+. The cyclic voltammetry (CV) curves of the Co_3O_4 powders formed from the Co-C composite powders reduced at 400 °C for the first five cycles at a scan rate of 0.1 mV s^{-1} are shown in Fig. 8a. The sharp reduction peak observed at 0.84 V in the first cathodic sweep was attributed to the conversion (faradic) reaction between Co_3O_4 and Li^+, which led to the formation of metallic Co and Li_2O [45]. The one broad oxidation peak observed at around 2.0 V was attributed to the oxidation of metallic Co to Co_3O_4 and the decomposition of Li_2O [46]. From the second cycle onward, the reduction peak shifted to a higher potential at around 1.1 V due to the conversion of Co_3O_4 crystals into the ultrafine nanocrystals during the first cycle [47]. The Co_3O_4 powders formed from the Co-C composite powders reduced at 400, 600, and 800 °C had similar shapes in their CV curves as shown in Fig. 8a and Fig. S3. The three samples also had similar shapes in their initial discharge and charge curves obtained at a current density of 1 A g^{-1} (Fig. 8b). The lithium-ion storage in the Co_3O_4 powders occurred by non-faradaic and faradaic reaction mechanisms [48]. The long plateau region in the initial discharge profile at a voltage of approximately 1 V was attributed to the faradaic reaction process. In addition, the pseudocapacitive process appears as a sloping voltage feature until the end of discharge [48]. The initial discharge capacities of the Co_3O_4 powders formed from the Co-C composite powders reduced at 400, 600, and 800 °C were 1033, 1099, and 1046 mA h g^{-1}, respectively, and their corresponding initial Coulombic efficiencies were 72, 75, and 76%, respectively. The high irreversible capacity loss during the first cycle of the transition metal oxide materials due to the irreversible structural damage and the formation of organic polymer film has been well known [49]. Degree of irreversibility during the first cycle has been effectively reduced by prelithiation of electrode material by Hassoun et al. [50]. Lopez et al. reported that the large irreversibility observed in the first discharge of crystalline oxides could be minimized by forming the thin film electrode [51]. The cycling performances of the three samples at a current density of 1 A g^{-1} are shown in Fig. 8c. The three samples had similar cycling performances irrespective of the Co_3O_4 hollow nanosphere size. The discharge capacities of the three samples were well maintained during the first 150 cycles, and then decreased slightly during the next 150 cycles. The discharge capacities of the Co_3O_4 powders formed from the Co-C composite powders reduced at 400, 600, and 800 °C for the 300th cycle were 644, 702, and 660 mA h g^{-1}, respectively, and their capacity retentions calculated from the second cycle were 81, 86, and 84%, respectively. The rate performances of the three samples are shown in Fig. 8d, in which the current density is increased step-wise from 0.5 to 10 A g^{-1}. The three samples had excellent rate performances and showed high capacities even at an extremely high current density of 10 A g^{-1}. However, the porous-structured Co_3O_4 powders formed from the Co-C composite powders reduced at 800 °C showed slightly better rate performance than those of the other two samples. The final discharge capacities of the Co_3O_4 powders formed from the Co-C composite powders reduced at 800 °C at current densities of 0.5, 1.5, 3, 5, 7, and 10 A g^{-1} were 830, 767, 715, 664, 621, and 581 mA h g^{-1}, respectively. The discharge capacities decreased slightly as the current density increased. Additionally, the three samples showed good capacity recovery properties when the current density returned to 0.5 A g^{-1}, even after cycling at high current densities.

Electrochemical impedance spectroscopy (EIS) measurements

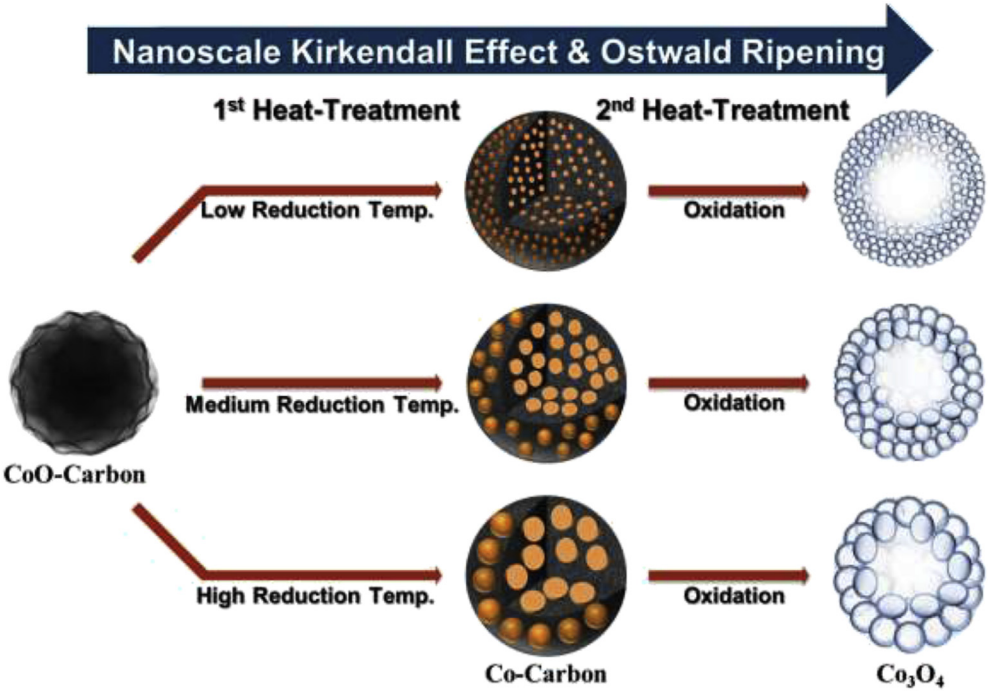

Scheme 1. Schematic diagram for the formation mechanism of the Co_3O_4 powders consisting of size controlled hollow nanospheres.

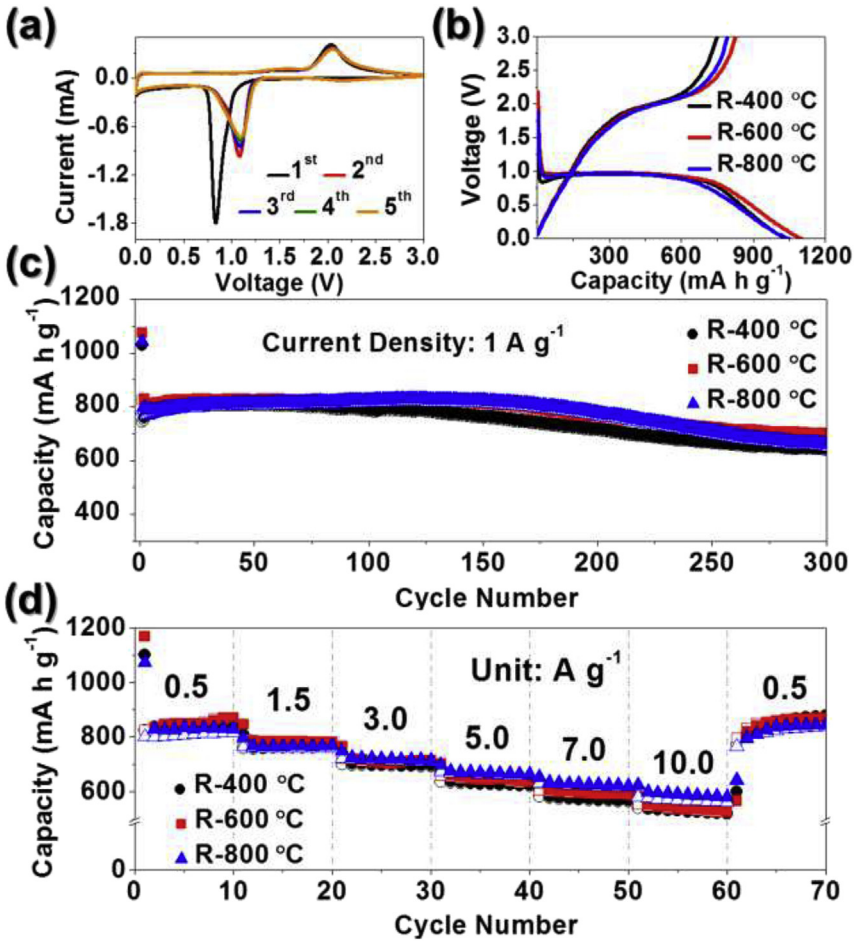

Fig. 8. Electrochemical properties of the Co_3O_4 powders with size controlled hollow nanospheres: (a) CV curves, (b) charge-discharge curves, (c) cycling performances, and (d) rate performances.

of the three samples before and after cycling were performed to explain their superior lithium-ion storage properties. The Nyquist plots shown in Fig. 9 reveal compressed semicircles in the medium-frequency range, which describe the charge-transfer resistance (R_{ct}) of the electrode [52,53]. The three samples had similar charge-transfer resistances after 50 cycles due to their similar structural stabilities during cycling. The SEM images shown in Fig. S4 reveal the morphologies of the three samples obtained after 50 cycles. The spherical morphologies of the three samples were well maintained after cycling, independent of the sizes of the Co_3O_4 hollow nanospheres present. The hollow structure of the micron-sized Co_3O_4 powders formed by Ostwald ripening accommodated the huge volume change during cycling. Additionally, the Co_3O_4 hollow nanospheres formed by nanoscale Kirkendall diffusion improved the stability of the internal structure of the micron-sized Co_3O_4 powders during cycling.

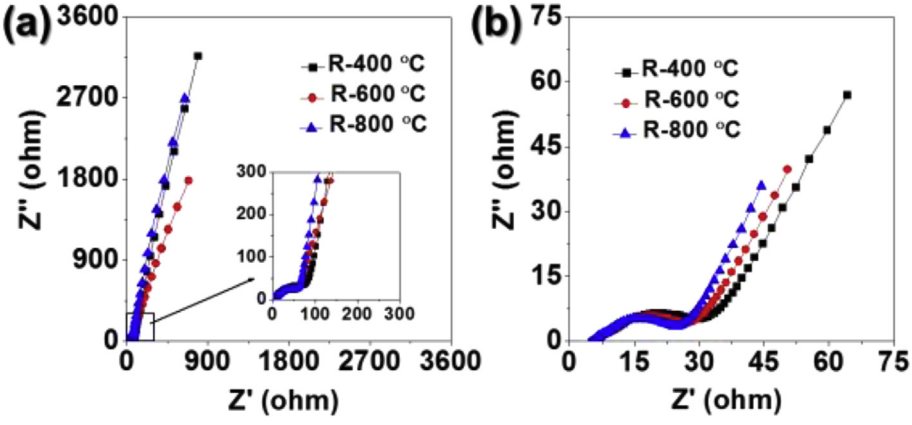

Fig. 9. Nyquist plots of the three samples (a) before and (b) after 50 cycles.

4. Conclusions

Micron-sized hollow powders consisting of size controlled Co_3O_4 hollow nanospheres were prepared by a second-step post-treatment process on CoO-C composite powders obtained by one-pot spray pyrolysis. Ostwald ripening during oxidation of the Co-C composite powders resulted in micron-sized powders with hollow structures. The shell region of the hollow powders consisted of ultrafine Co_3O_4 hollow nanospheres formed by nanoscale Kirkendall effects during oxidation of metallic Co nanocrystals. The mean sizes of the ultrafine Co_3O_4 hollow nanospheres were determined by the mean sizes of the metallic Co nanocrystals uniformly dispersed within the carbon matrix. The micron-sized hollow powders showed excellent lithium-ion storage performances independent of nanosphere size. The strategy developed in this study could be efficiently applied in the preparation of micron-sized hollow metal oxide powders consisting of ultrafine hollow nanospheres for a number of different applications, including energy storage.

Acknowledgment

This work was supported by a National Research Foundation of Korea grant funded by the Korea government (MEST) (NRF-2015R1A2A1A15056049). This work was supported by the Energy Efficiency & Resources Core Technology Program of the Korea Institute of Energy Technology Evaluation and Planning, granted financial resource from the Ministry of Trade, Industry & Energy, Republic of Korea (201320200000420 and 20153030091450).

Appendix A. Supplementary data

Supplementary data related to this article can be found at http://dx.doi.org/10.1016/j.jallcom.2016.07.233.

References

[1] Q. Li, P. Wang, Q. Feng, M. Mao, J. Liu, H. Wang, S.X. Mao, X.X. Zhang, Superior flexibility of a wrinkled carbon shell under electrochemical cycling, J. Mater. Chem. A 2 (2014) 4192–4197.
[2] M. Wang, D. Xue, H. Qin, L. Zhang, G. Ling, J. Liu, Y. Fang, L. Meng, Preparation of FeS_2 nanotube arrays based on layer-by-layer assembly and their photoelectrochemical properties, Mater. Sci. Eng. B Solid 204 (2016) 38–44.
[3] Z. Yuan, L. Si, X. Zhu, Three-dimensional hard carbon matrix for sodium-ion battery anode with superior-rate performance and ultralong cycle life, J. Mater. Chem. A 3 (2015) 23403–23411.
[4] B. Guo, K. Yu, H. Li, H. Song, Y. Zhang, X. Lei, H. Fu, Y. Tan, Z. Zhu, Hollow structured micro/nano MoS_2 spheres for high electrocatalytic activity hydrogen evolution reaction, ACS Appl. Mater. Interfaces 8 (2016) 5517–5525.
[5] R. Wu, X. Qian, F. Yu, H. Liu, K. Zhou, J. Wei, Y.J. Huang, MOF-templated formation of porous CuO hollow octahedra for lithium-ion battery anode materials, J. Mater. Chem. A 1 (2013) 11126–11129.
[6] R. Wu, X. Qian, K. Zhou, J. Wei, J. Lou, P.M. Ajayan, Porous spinel $Zn_xCo_{3-x}o_4$ hollow polyhedra templated for high-rate lithium-ion batteries, ACS Nano 8 (2014) 6297–6303.
[7] J.S. Han, D.Y. Chung, D.G. Ha, J.H. Kim, K. Choi, Y.E. Sung, S.H. Kang, Nitrogen and boron Co-Doped hollow carbon catalyst for the oxygen reduction reaction, Carbon 105 (2016) 1–7.
[8] Z. Zhang, G. Wang, Y. Lai, J. Li, A freestanding hollow carbon nanofiber/reduced graphene oxide interlayer for high-performance lithium–sulfur batteries, J. Alloys Compd. 663 (2016) 501–506.
[9] L. Wang, Z. Lou, J. Deng, R. Zhang, T. Zhang, Ethanol gas detection using a yolk-shell (Core-Shell) α-Fe_2O_3 nanospheres as sensing material, ACS Appl. Mater. Interfaces 7 (2015) 13098–13104.
[10] J. Liu, Z. Yang, J. Wang, L. Gu, J. Maier, Y. Yu, Three-dimensionally interconnected nickel-antimony intermetallic hollow nanospheres as anode material for high-rate sodium-ion batteries, Nano Energy 16 (2015) 389–398.
[11] H.B. Zeng, W.P. Cai, P.S. Liu, X.X. Xu, H.J. Zhou, C. Klingshirn, H. Kalt, ZnO-based hollow nanoparticles by selective etching: elimination and reconstruction of metal–semiconductor interface, improvement of blue emission and photocatalysis, ACS Nano 2 (2008) 1661–1670.
[12] S.M. Zhou, D.K. Ma, S.H. Zhang, W. Wang, W. Chen, S.M. Huang, K. Yu, PEGylated Cu_3BiS_3 hollow nanospheres as a new photothermal agent for 980 nm-laser-driven photothermochemotherapy and a contrast agent for x-ray computed tomography imaging, Nanoscale 8 (2016) 1374–1382.
[13] W.S. Kim, Y. Hwa, H.C. Kim, J.H. Choi, H.J. Sohn, S.H. Hong, SnO_2@Co_3O_4 hollow nano-spheres for a Li-Ion battery anode with extraordinary performance, Nano Res. 7 (2014) 1128–1136.
[14] M. Sasidharan, N. Gunawardhana, C. Senthil, M. Yoshio, Micelle templated NiO hollow nanospheres as anode materials in lithium ion batteries, J. Mater. Chem. A 2 (2014) 7337–7344.
[15] Y. Lee, M.R. Jo, K. Song, K.M. Nam, J.T. Park, Y.M. Kang, Hollow Sn–SnO_2 nanocrystal/graphite composites and their lithium storage properties, ACS Appl. Mater. Interfaces 4 (2012) 3459–3464.
[16] D.Y. Chen, G. Ji, Y. Ma, J.Y. Lee, J.M. Lu, Graphene-encapsulated hollow Fe_3O_4 nanoparticle aggregates as a high-performance anode material for lithium ion batteries, ACS Appl. Mater. Interfaces 3 (2011) 3078–3083.
[17] D. Deng, J.Y. Lee, Hollow core–shell mesospheres of crystalline SnO_2 nanoparticle aggregates for high capacity Li+ ion storage, Chem. Mater 20 (2008) 1841–1846.
[18] H. Guo, R. Mao, D. Tian, W. Wang, D. Zhao, X. Yang, S. Wang, Morphology-controlled synthesis of SnO_2/C hollow core–shell nanoparticle aggregates with improved lithium storage, J. Mater. Chem. A 1 (2013) 3652–3658.
[19] K. Hadinoto, P. Phanapavudhikul, Z. Kewu, R.B. Tan, Novel formulation of large hollow nanoparticles aggregates as potential carriers in inhaled delivery of nanoparticulate drugs, Ind. Eng. Chem. Res. 45 (2006) 3697–3706.
[20] Z. Liu, D.D. Sun, P. Guo, J.O. Leckie, One-step fabrication and high photocatalytic activity of porous TiO_2 hollow aggregates by using a low-temperature hydrothermal method without templates, Chem. Eur. J. 13 (2007) 1851–1855.
[21] S. Elhag, Z.H. Ibupoto, X. Liu, O. Nur, M. Willander, Dopamine wide range detection sensor based on modified Co_3O_4 nanowires electrode, Sens. Actuators B 203 (2014) 543–549.
[22] H. Jin, J. Wang, D. Su, Z. Wei, Z. Pang, Y. Wang, In situ cobalt–cobalt oxide/N-doped carbon hybrids as superior bifunctional electrocatalysts for hydrogen and oxygen evolution, J. Am. Chem. Soc. 137 (2015) 2688–2694.
[23] R.R. Salunkhe, J. Tang, Y. Kamachi, T. Nakato, J.H. Kim, Y. Yamauchi, Asymmetric supercapacitors using 3D nanoporous carbon and cobalt oxide electrodes synthesized from a single metal–organic framework, ACS Nano 9 (2015) 6288–6296.
[24] G.S. Hutchings, Y. Zhang, J. Li, B.T. Yonemoto, X. Zhou, K. Zhu, F. Jiao, In situ formation of cobalt oxide nanocubanes as efficient oxygen evolution catalysts, J. Am. Chem. Soc. 137 (2015) 4223–4229.
[25] S.J. Hwang, K.I. Choi, J.W. Yoon, Y.C. Kang, J.H. Lee, Pure and palladium-loaded Co_3O_4 hollow hierarchical nanostructures with giant and ultraselective chemiresistivity to xylene and toluene, Chem. Eur. J. 21 (2015) 5872–5878.
[26] C. Yan, G. Chen, X. Zhou, J. Sun, C. Lv, Template-based engineering of carbon-doped Co_3O_4 hollow nanofibers as anode materials for lithium-ion batteries, Adv. Funct. Mater 26 (2016) 1428–1436.
[27] P. Poizot, S. Laruelle, S. Grugeon, L. Dupont, J.M. Tarascon, Nano-sized transition-metal oxides as negative-electrode materials for lithium-ion batteries, Nature 407 (2000) 496–499.
[28] L. Peng, Y. Feng, Y. Bai, H.J. Qiu, Y. Wang, Designed synthesis of hollow Co_3O_4 nanoparticles encapsulated in a thin carbon nanosheet array for high and reversible lithium storage, J. Mater. Chem. A 3 (2015) 8825–8831.
[29] H. Wang, N. Mao, J. Shi, Q. Wang, W. Yu, X. Wang, Cobalt oxide-carbon nanosheet nanoarchitecture as an anode for high-performance lithium-ion battery, ACS Appl. Mater. Interfaces 7 (2015) 2882–2890.
[30] Y.M. Chen, L. Yu, X.W.D. Lou, Hierarchical tubular structures composed of Co_3O_4 hollow nanoparticles and carbon nanotubes for lithium storage, Angew. Chem. Int. Ed. 55 (2016) 5990–5993.
[31] N. Du, H. Zhang, B.D. Chen, J.B. Wu, X.Y. Ma, Z.H. Liu, Y.Q. Zhang, D. Yang, X.H. Huang, J.P. Tu, Porous Co_3O_4 nanotubes derived from $Co_4(CO)_{12}$ clusters on carbon nanotube templates: a highly efficient material for Li-Battery applications, Adv. Mater. 19 (2007) 4505–4509.
[32] Y. Han, M. Zhao, L. Dong, J. Feng, Y. Wang, D. Li, X. Li, MOF-derived porous hollow Co_3O_4 parallelepipeds for building high-performance Li-Ion batteries, J. Mater. Chem. A 3 (2015) 22542–22546.
[33] J. Yang, H.J. Qiu, L. Peng, W. Li, Y. Wang, Unique synthesis of hollow Co_3O_4 nanoparticles embedded in thin Al_2O_3 nanosheets for enhanced lithium storage, Nanoscale 7 (2015) 15983–15989.
[34] X. Wang, X.L. Wu, Y.G. Guo, Y. Zhong, X. Cao, Y. Ma, J. Yao, Synthesis and Lithium Storage Properties of Co3O4 nanosheet-assembled multishelled hollow spheres, Adv. Funct. Mater. 20 (2010) 1680–1686.
[35] G.D. Park, J.H. Lee, J.K. Lee, Y.C. Kang, Effect of esterification reaction of citric acid and ethylene glycol on the formation of multi-shelled cobalt oxide powders with superior electrochemical properties, Nano Res. 7 (2014) 1738–1748.
[36] G.D. Park, J.S. Cho, Y.C. Kang, Novel cobalt oxide-nanobubble-decorated reduced graphene oxide sphere with superior electrochemical properties prepared by nanoscale Kirkendall diffusion process, Nano Energy 17 (2015) 17–26.
[37] Y.J. Hong, J.S. Cho, Y.C. Kang, Superior electrochemical properties of nanofibers composed of hollow $CoFe_2O_4$ nanospheres covered with onion-like graphitic carbon, Chem. Eur. J. 21 (2015) 18202–18208.
[38] J.S. Cho, Y.J. Hong, Y.C. Kang, Design and synthesis of bubble-nanorod-structured Fe_2O_3–Carbon nanofibers as advanced anode material for Li-Ion batteries, ACS Nano 9 (2015) 4026–4035.

[39] J.S. Cho, J.M. Won, J.H. Lee, Y.C. Kang, Synthesis and electrochemical properties of spherical and hollow-structured NiO aggregates created by combining the Kirkendall effect and Ostwald ripening, Nanoscale 7 (2015) 19620–19626.
[40] W.S. Wang, L. Zhen, C.Y. Xu, W.Z. Shao, Z.L. Chen, formation of $CdMoO_4$ porous hollow nanospheres via a self-assembly accompanied with Ostwald ripening process and their photocatalytic performance, CrystEngComm 15 (2013) 8014–8021.
[41] W.S. Wang, L. Zhen, C.Y. Xu, B.Y. Zhang, W.Z. Shao, Room temperature synthesis of hollow $CdMoO_4$ microspheres by a surfactant-free aqueous solution route, J. Phys. Chem. B 110 (2006) 23154–23158.
[42] H.J. Song, X.H. Jia, H. Qi, X.F. Yang, H. Tang, C.Y. Min, Flexible morphology-controlled synthesis of monodisperse a-Fe_2O_3 hierarchical hollow microspheres and their gas-sensing properties, J. Mater. Chem. 22 (2012) 3508–3516.
[43] D.H. Ha, L.M. Moreau, S. Honrao, R.G. Hennig, R.D. Robinson, The oxidation of cobalt nanoparticles into kirkendall-hollowed CoO and Co_3O_4: the diffusion mechanisms and atomic structural transformations, J. Mater. Chem. A 2 (2014) 7337–7344.
[44] Y. Xiao, S. Liu, S. Fang, D. Jia, H. Su, W. Zhou, J.B. Wiley, F. Li, Plum-like and octahedral Co_3O_4 single crystals on and around carbon nanotubes: large scale synthesis and formation mechanism, RSC Adv. 2 (2012) 3496–3501.
[45] X. Yao, X. Xin, Y. Zhang, J. Wang, Z. Liu, X. Xu, Co_3O_4 nanowires as high capacity anode materials for lithium ion batteries, J. Alloys Compd. 521 (2012) 95–100.
[46] D. Larcher, G. Sudant, J.B. Leriche, Y. Chabre, J.M. Tarascon, The electrochemical reduction of Co_3O_4 in a lithium cell, J. Electrochem. Soc. 149 (2002) A234–A241.
[47] H.J. Liu, S.H. Bo, W.J. Cui, F. Li, C.X. Wang, Y.Y. Xia, Nano-sized cobalt oxide/mesoporous carbon sphere composites as negative electrode material for lithium-ion batteries, Electrochim. Acta 53 (2008) 6497–6503.
[48] C. Vidal-Abarca, P. Lavela, J.L. Tirado, A ^{57}Fe mossbauer spectroscopy study of cobalt ferrite conversion electrodes for Li-Ion batteries, J. Power Sources 196 (2011) 6978–6981.
[49] S. Grugeon, S. Laruelle, R. Herrera-Urbina, L. Dupont, P. Poizot, J.-M. Tarascon, Particle size effects on the electrochemical performance of copper oxides toward lithium, J. Electrochem. Soc. 148 (2001) A285–A292.
[50] J. Hassoun, K.S. Lee, Y.-K. Sun, B. Scrosati, An advanced lithium ion battery based on high performance electrode materials, J. Am. Chem. Soc. 133 (2011) 3139–3143.
[51] M.C. López, G.F. Ortiz, P. Lavela, R. Alcántara, J.L. Tirado, Improved energy storage solution based on hybrid oxide materials, ACS Sustain. Chem. Eng. 1 (2013) 46–56.
[52] N. Li, G. Liu, C. Zhen, F. Li, L. Zhang, H.M. Cheng, Battery performance and photocatalytic activity of mesoporous anatase TiO_2 nanospheres/graphene composites by template-free self-assembly, Adv. Funct. Mater. 21 (2011) 1717–1722.
[53] X. Du, W. He, X. Zhang, Y. Yue, H. Liu, X. Zhang, D. Min, X. Ge, Y. Du, Enhancing the electrochemical performance of lithium ion batteries using mesoporous $Li_3V_2(PO_4)_3$/C microspheres, J. Mater. Chem. 22 (2012) 5960–5969.